Experimental validation of Mach-Zehnder Interferometer group index by measuring free spectral range

Matthew Koecher

Abstract Silicon photonics provides a method for creating optical circuits using silicon and electronics manufacturing techniques. One important component is the Mach-Zehnder Interferometer (MZI). In this paper we propose determining the group index of manufactured MZI by measuring the Free Spectral Range (FSR) and calculating the group index

1 Introduction

A Mach-Zehnder Interferometer consists of a waveguide that is split into two paths, which can be equal in length (balanced), or unequal in length (unbalanced). The two paths are coupled together again and the light that is propagated depends on the relative lengths of the two arms of the MZI.

2 Waveguide

We first use Lumerical MODE to derive the properties of the silicon waveguide. Our waveguides will be 220nm in height and 500nm in width to support single-mode propagation. In addition, we use TE-polarized grating couplers to couple the light on and off the chip.

Lumerical MODE computes the field intensity for our waveguides, and this is shown in Figure 1.

Next we compute a compact model for the waveguide that can be used for later circuit simulations. This is done by sweeping a spectral range for the effective index, then fitting a polynomial expression to this curve. Figure shows a plot of effective index from 1.5 micron to
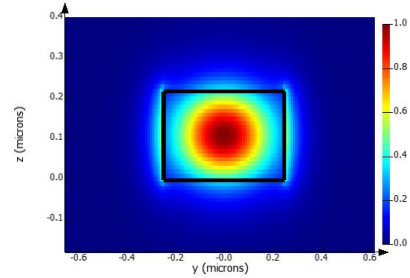
Matthew Koecher
Affiliation not available

Fig. 1 Field intensity in waveguide

1.6 micron, and the following equation shows the polynomial fit.
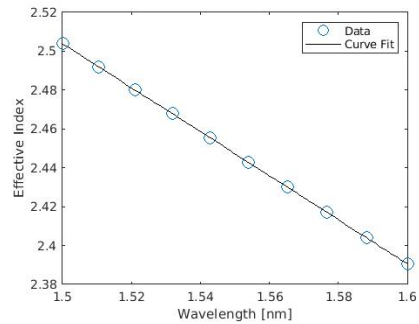

Fig. 2 Wavelength sweep of Effective Index

$$n_{eff}(\lambda) = 2.4 - 1.1(\lambda - 1.55) - 0.1(\lambda - 1.55)^2$$

4 Mach-Zehnder Interferometer

The basic layout of a MZI is shown in figure 3. Incoming light is split into two branches. For the unbalanced MZI, these branches have different lengths. The light is coupled together at the end. For frequencies that experience a π phase shift from the different lengths, those frequencies will destructively interfere and the light radiates out of the waveguide.
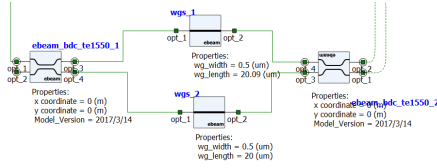

Fig. 3 MZI Schematic from Lumerical INTERCONNECT

Light is modeled as a plane wave as describe by the following equation:

$E = E_0 e^{i(\omega t - \beta z)}$

where

$\beta = \frac{2\pi n}{\lambda}$

At the splitter, half of the light is directed down each branch. The light propagates down each branch, and the combined field is

$E_o = \frac{1}{\sqrt{2}} \left(E_{o1} + E_{o2} \right) = \frac{E_i}{2} \left(e^{-i\beta_1 L_1 - \frac{\alpha_1}{2} L_1} + e^{-i\beta_2 L_2 - \frac{\alpha_2}{2} L_2} \right)$

Converting the E-field to intensity, and assuming loss-less propagation, this simplifies to:

$\frac{I_o}{I_i} = \frac{1}{2} \left[1 + \cos \left(\beta \Delta L \right) \right]$

FSR is defined as the space between adjacent peaks, or where the phase shift is a multiple of 2π.

Solving for FSR gives

$FSR = \Delta\lambda = \frac{\lambda^2}{\Delta L n_g}$

5 Simulation

Table 1 shows the devices that will be fabricated. FSR were calculated using Lumerical INTERCONNECT simulations. In addition, a de-embedding device is included which includes just an input grating coupler, and a Y-Branch connection to two output grating couplers. From this device we can learn the response of the grating couplers themselves.

The included figures show the simulated gain response of the MZI devices as calculated in Lumerical INTERCONNECT.

Monte-Carlo simulations were run to take into account manufacturing variability. [1] For this purpose, 50 simulations were run on each MZI, and the resulting FSR binned into histograms.

Delta L (nm)	FSR (nm)
0	N/A
30	18.3
100	5.5
400	1.4

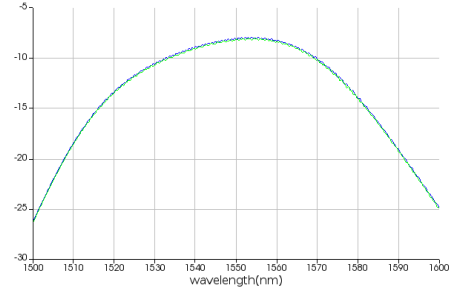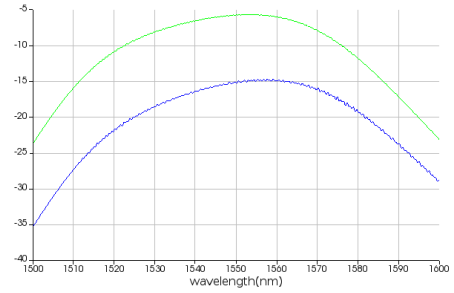**Table 1** List of MZI device lengths and their associated FSR

Fig. 4 Direct Grating Coupler Connection
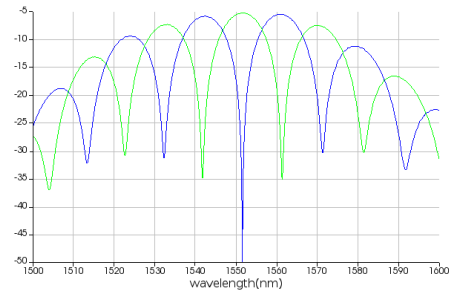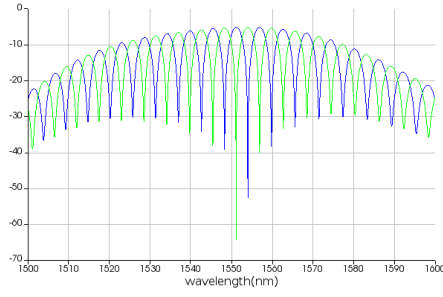
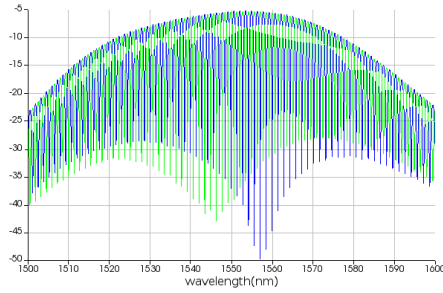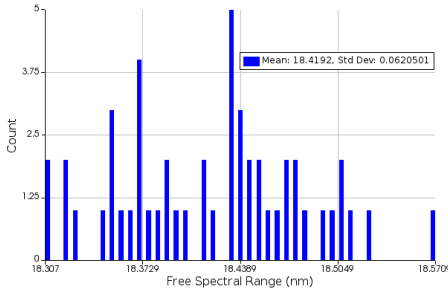

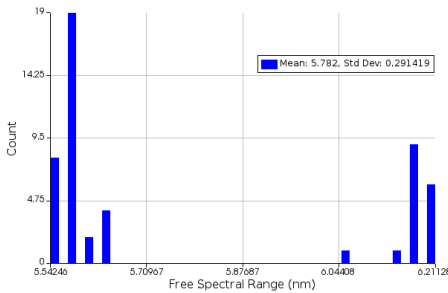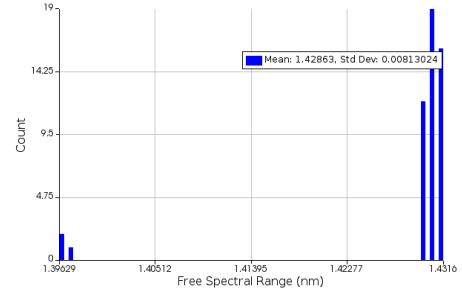**Fig. 5** Balanced MZI, Δ L $= 0$

Fig. 6 ΔL $= 30$

Table 2 shows the data from the simulation runs. The group index is calculated from the FSR histogram bins.

6 Fabrication

Fig. 7 ΔL = 100

Fig. 8 ΔL = 400

Fig. 9 Monte-Carlo histogram, MZI ΔL = 30 nm

Fig. 10 Monte-Carlo histogram, MZI ΔL = 100 nm

Fig. 11 Monte-Carlo histogram, MZI ΔL = 400 nm

Delta L	FSR			Group Index		
	Min	Max	Mean	Max	Min	Mean
30	18.31	18.57	18.42	4.37	4.31	4.35
100	5.54	6.21	5.78	4.34	3.87	4.16
400	1.4	1.43	1.42	4.3	4.19	4.22

Table 2 Fabrication variances from Monte-Carlo Simulations

The devices were fabricated using 100 keV Electron Beam Lithography [2]. The fabrication used silicon-on-insulator wafer with 220 nm thick silicon on 3 μm thick silicon dioxide. The substrates were 25 mm squares diced from 150 mm wafers. After a solvent rinse and hot-plate dehydration bake, hydrogen silsesquioxane re-

sist (HSQ, Dow-Corning XP-1541-006) was spin-coated at 4000 rpm, then hotplate baked at 80 °C for 4 minutes. Electron beam lithography was performed using a JEOL JBX-6300FS system operated at 100 keV energy, 8 nA beam current, and 500 μm exposure field size. The machine grid used for shape placement was 1 nm, while the beam stepping grid, the spacing between dwell points during the shape writing, was 6 nm. An exposure dose of 2800 μC/cm2 was used. The resist was developed by immersion in 25% tetramethylammonium hydroxide for 4 minutes, followed by a flowing deionized water rinse for 60 s, an isopropanol rinse for 10 s, and then blown dry with nitrogen. The silicon was removed from unexposed areas using inductively coupled plasma etching in an Oxford Plasmalab System 100, with a chlorine gas flow of 20 sccm, pressure of 12 mT, ICP power of 800 W, bias power of 40 W, and a platen temperature of 20 °C, resulting in a bias voltage of 185 V. During etching, chips were mounted on a 100 mm silicon carrier wafer using perfluoropolyether vacuum oil. Cladding oxide was deposited using plasma enhanced chemical vapor deposition (PECVD) in an Oxford Plasmalab System 100 with a silane (SiH4) flow of 13.0 sccm, nitrous oxide (N2O) flow of 1000.0 sccm, high-purity nitrogen (N2) flow of 500.0 sccm, pressure at 1400mT, high-frequency RF power of 120W, and a platen temperature of 350C. During deposition, chips rest directly on a silicon carrier wafer and are buffered by silicon pieces on all sides to aid uniformity.[3]

6.1 Device Characterization

To characterize the devices, a custom-built automated test setup [4]with automated control software written in Python was used [5]. An Agilent 81600B tunable laser was used as the input source and Agilent 81635A optical power sensors as the output detectors. The wavelength was swept from 1500 to 1600 nm in 10 pm steps. A polarization maintaining (PM) fibre was used to maintain the polarization state of the light, to couple the TE polarization into the grating couplers [6]. A 90º rotation was used to inject light into the TM grating couplers [6]. A polarization maintaining fibre array was used to couple light in/out of the chip [7].

6.2 Acknowledgments:

7 Analysis

The goal of analysis is to find the group index of the manufactured device and compare that to the results found in simulation. To do this, we must first determine the parameters of the MZI based on the measured data.

First step is to remove the response of the grating couplers so we can see the effect of the MZI itself. For example, Figure 12 shows the measured data of a de-embedding device: one input GC followed by a Y-branch which connects to two output GC. As can be seen, the response peaks around 1600 nm.

In Figure 13 the raw measured data for one of the MZI devices is plotted. The characteristic response of the GC can be seen superimposed on the MZI peaks. To compensate for this, a low-order polynomial is fit to the data, then subtracted from it. The results are seen in Figure 14.
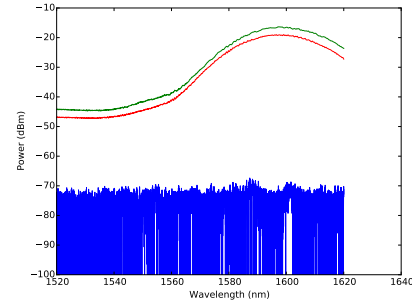

Fig. 12 ng couplers so we can see the effect of the MZI itself. For example, Figure 12 shows the measured data of a de-embedding device: one input GC followed by a Y-branch which connects to two output GC. As can be seen, the response peaks just below 1600 nm. De-embedding structures to show the response of the grating couplers
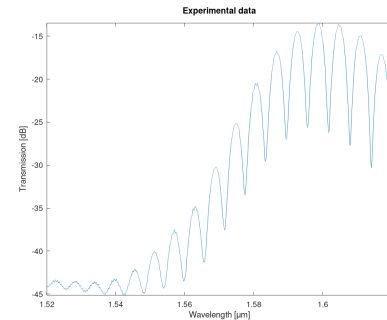

Fig. 13 Raw measured data for MZI with ΔL=100nm

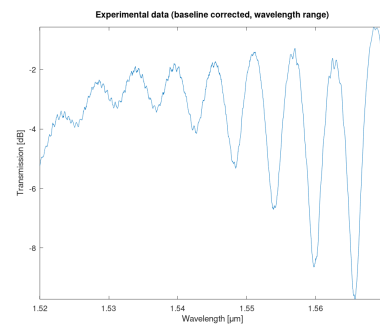

Fig. 14 Baseline correction applied to MZI with ΔL=100nm

From here, the peaks are found using the MATLAB "findpeaks" routine. The distance between peaks determines the FSR, which in turn can be used to find the group index. Figure 15 shows the plot of the MZI

function that has been fit to the measured data. It can be determined the the group index of this MZI is 4.21.

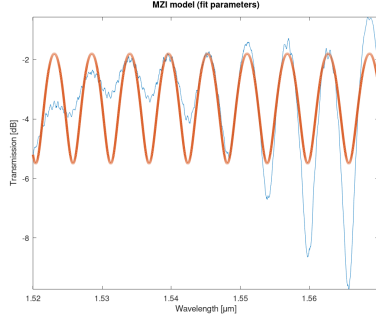Figures 16-19 show plots from other MZI devices, with ΔL from 30 to 400 nm.

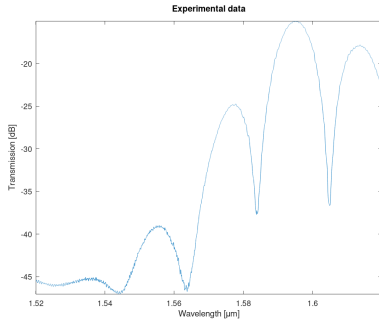**Fig. 15** MZI with ΔL=100nm with parameters fit from the measured data

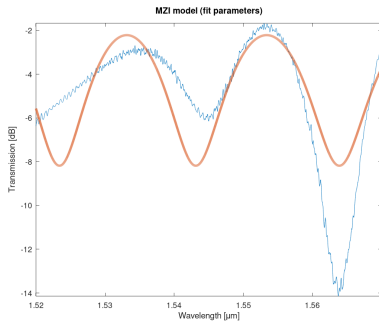**Fig. 16** Raw measured data for MZI with ΔL=30nm

Fig. 17 MZI with ΔL=30nm with parameters fit from the measured data

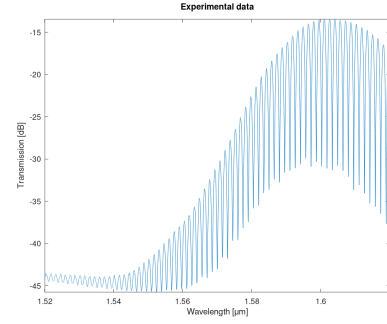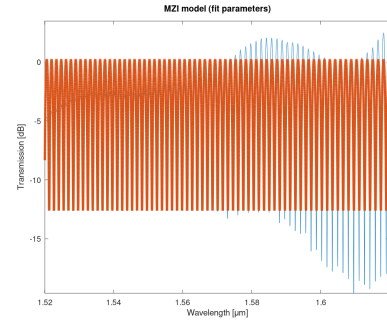**Fig. 18** Raw measured data for MZI with ΔL=400nm

Fig. 19 MZI with ΔL=400nm with parameters fit from the measured data

Table 3 shows a summary of the FSR and group index calculated from the measured data. Comparing with the Monte-Carlo simulations above, we can see that the 100 nm devices do fall within the predicted range from the simulations, but the 30 nm and 400 nm devices fall just outside the range.

Delta L	N_G	FSR
100	4.21	5.86
100A	4.18	5.99
30	4.25	19.6
400	4.17	1.5

Table 3 FSR and Group Index calculated from measured data

8 Conclusion

This work shows the derivation of a Mach-Zehnder interferometer transfer function, which was used to simulate performance for several different devices with unbalanced lengths. These devices were fabricated, and

the measured data compared to the simulations. It was determined that some devices did indeed fall within the predicted values of the simulations, while others were close but outside the predicted range.

References

1. (2017) Performance prediction for silicon photonics integrated circuits with layout-dependent correlated manufacturing variability. Optics Express

2. (2011) Electron beam lithography writing strategies for low loss, high confinement silicon optical waveguides. J Vacuum Sci Technol B 29, 06F309

3. Phot1x course on edX

4. Maple Leaf Photonics

5. `http://siepic.ubc.ca/probestation`, using Python code developed by Michael Caverley

6. (2014) Focusing sub-wavelength grating couplers with low back reflections for rapid prototyping of silicon photonic circuits. Optics Express 22:

7. www.plcconnections.com, PLC Connections, Columbus OH, USA

8. Chrostowski L, Hochberg M (2015) Silicon Photonics Design. Cambridge University Press (CUP)

9. Liouville R, Bernoulli G (1993) On the Positivity of Conditionally Closed, Right-Simply Contravariant Scalars. Journal of Numerical Geometry 6:152–191

10. Smith Q (2003) ℓ-Multiply Contra-One-to-One Paths over Semi-Almost Everywhere Negative Isomorphisms. Journal of Homological Model Theory 7:1408–1423

11. Tate Q, Garcia L, Banach G (1995) Regularity Methods in Fuzzy Number Theory. Archives of the Moldovan Mathematical Society 0:78–93

12. Pepe A, Kurtz MJ (2012) A Measure of Total Research Impact Independent of Time and Discipline. PLoS ONE 7:e46428. `https://doi.org/10.1371/journal.pone.0046428`

13. Aad I, Castelluccia C (2001) Differentiation mechanisms for IEEE 802.11. In: Proceedings IEEE INFOCOM 2001. Conference on Computer Communications. Twentieth Annual Joint Conference of the IEEE Computer and Communications Society (Cat. No.01CH37213). Institute of Electrical and Electronics Engineers, pp 209–218

14. Bojko RJ, Li J, He L, et al. (2011) Electron beam lithography writing strategies for low loss high confinement silicon optical waveguides. Journal of Vacuum Science & Technology B: Microelectronics and Nanometer Structures 29:06F309. `https://doi.org/10.1116/1.3653266`

15. Chrostowski L, Hochberg M Testing and packaging. In: Silicon Photonics Design. Cambridge University Press (CUP), pp 381–405

16. Wang Y, Wang X, Flueckiger J, et al. (2014) Focusing sub-wavelength grating couplers with low back reflections for rapid prototyping of silicon photonic circuits. Opt Express 22:20652. `https://doi.org/10.1364/oe.22.020652`